Ionization of He by C^{6+}, $\overline{C}^{6-}$, e^-, and e^+

H. R. J. Walters[1] and Colm T. Whelan[2]

[1]*Centre for Theoretical Atomic, Molecular, and Optical Physics, School of Mathematics and Physics, Queen's University, Belfast BT7 1NN, United Kingdom*

[2]*Department of Physics, Old Dominion University, Norfolk, Virginia 23529-0116, USA*

(Received 11 May 2012; published 5 June 2012)

A recent theoretical paper [Colgan *et al.*, J. Phys. B **44**, 175205 (2011)] has reopened the problem of C^{6+} ionization of He at 100 MeV/amu. The issue concerns ionization in the plane perpendicular to the momentum transfer **q** for the case where the ejected electron has an energy of 6.5 eV and $q = 0.75$ a.u. Here, even after deconvolution, experiment finds two peaks near 90° and 270°, contrary to earlier theoretical works that had predicted dips. Now, Colgan *et al.* also find peaks. We have reinvestigated the problem using the second Born approximation whose results are supported by a nonperturbative impact-parameter coupled-pseudostate approximation. Dips are again predicted. By comparing C^{6+} impact with that of its antiparticle $\overline{C}^{6-}$ a "mirror-image" situation is observed in which the dips are converted into peaks, i.e., positively (negatively) charged projectiles give dips (peaks) near 90° and 270°. A physical interpretation of this result is suggested. Applying exactly the same second Born approximation to $e^{\pm}$ impact ionization of He at 1 keV under similar dynamical conditions to C^{6+}, we see exactly the same patterns, but now the results for e^-, showing peaks near 90° and 270° in the plane perpendicular to **q**, are in quite good agreement with experiment in this and other geometries. This is strong support for the predictions of the second Born approximation for C^{6+}. A paper by Egodapitiya *et al.* [Phys. Rev. Lett. **106**, 153202 (2011)] warns of coherence problems with heavy-particle beams. It is suggested that this, together with experimental resolutions, may explain the experimental data for C^{6+}.

DOI: 10.1103/PhysRevA.85.062701 PACS number(s): 34.50.Fa, 52.20.Hv

I. INTRODUCTION

In a previous publication McGovern *et al.* [1] made a detailed theoretical investigation of a serious discrepancy between theory and experiment concerning single ionization of He by C^{6+} observed in a plane (approximately) perpendicular to the momentum transfer vector. Although they also looked at other energies, the primary focus was on ionization by 100 MeV/amu C^{6+} with ejection of a 6.5 eV electron and a momentum transfer $q = 0.75$ a.u. Here, experiment saw two pronounced peaks near 90° and 270° in the triple (fully) differential cross section (TDCS) as the angle of observation was rotated in the perpendicular plane, see Fig. 2(f). By contrast, theoretical calculations in a variety of approximations [2–5], including the continuum distorted wave (CDW) approximation [4], had yielded shallow minima at these angles with shallow maxima at 0° (=360°) and 180°; see Fig. 2(f). Of course, experiments do not measure at precise angles and energies and experimental uncertainties need to be taken into account. This was done by Fiol *et al.* [4], who got agreement with experiment using both the first Born and CDW approximations. However, in a different analysis of experimental uncertainties, Dürr *et al.* [6] concluded that the observed peaks could only be explained in part by experimental resolutions and that, consequently, there existed a substantive discrepancy between theory and experiment in this perpendicular plane geometry. To account for this discrepancy Schulz and coworkers [2,7,8] advanced a theory in which the C^{6+} first ionizes the electron and then scatters elastically off the recoil ion (essentially the target nucleus). In this model the two scatterings are combined incoherently, whereas a proper quantum-mechanical treatment would require them to be added coherently. Further, it is assumed that ionization is always followed by elastic scattering, i.e., the probability of elastic scattering is unity. Quantum scattering theory admits no such certainty; see Sec. II A. This elastic scattering model, together with the treatment of experimental resolutions, seemed to explain most of the previously observed differences between theory and experiment [7,8].

In [1] McGovern *et al.* ruled out the elastic scattering model by showing that a second Born treatment of the collision, which explicitly includes elastic scattering of C^{6+} by the target nucleus but in a proper coherent quantum-mechanical way, was in accord with the earlier theoretical works and, in particular, with a sophisticated nonperturbative impact-parameter coupled-pseudostate (CP) approximation [5]; see Fig. 1. This latter also coherently incorporates elastic scattering of C^{6+} by the target nucleus. A significant discrepancy between theory and experiment therefore still existed. However, other possibilities had been neglected in previous theoretical work, and so McGovern *et al.* [1] proceeded to rule these out. Thus, they went on to show that the quality of electronic bound and continuum wave functions in their calculations was not an issue, that there was negligible contribution at 100 MeV/amu from collisions in which the He^+ is left in an excited state (although at lower energies such as 2 MeV/amu this could be significant), and that, while 100 MeV/amu is inside the relativistic domain (impact velocity $= 0.46c$), the pattern of the theoretical results should not be altered substantively by relativistic effects.

At the end of [1] it was clear that a conflict between theory and experiment still remained. However, the problem has been reopened by a recent theoretical paper by Colgan *et al.* [9] which gets agreement with the positions of the peaks seen in experiment but not in their magnitude. Colgan *et al.* have examined the problem using an impact-parameter time-dependent close-coupling (TDCC) approximation both

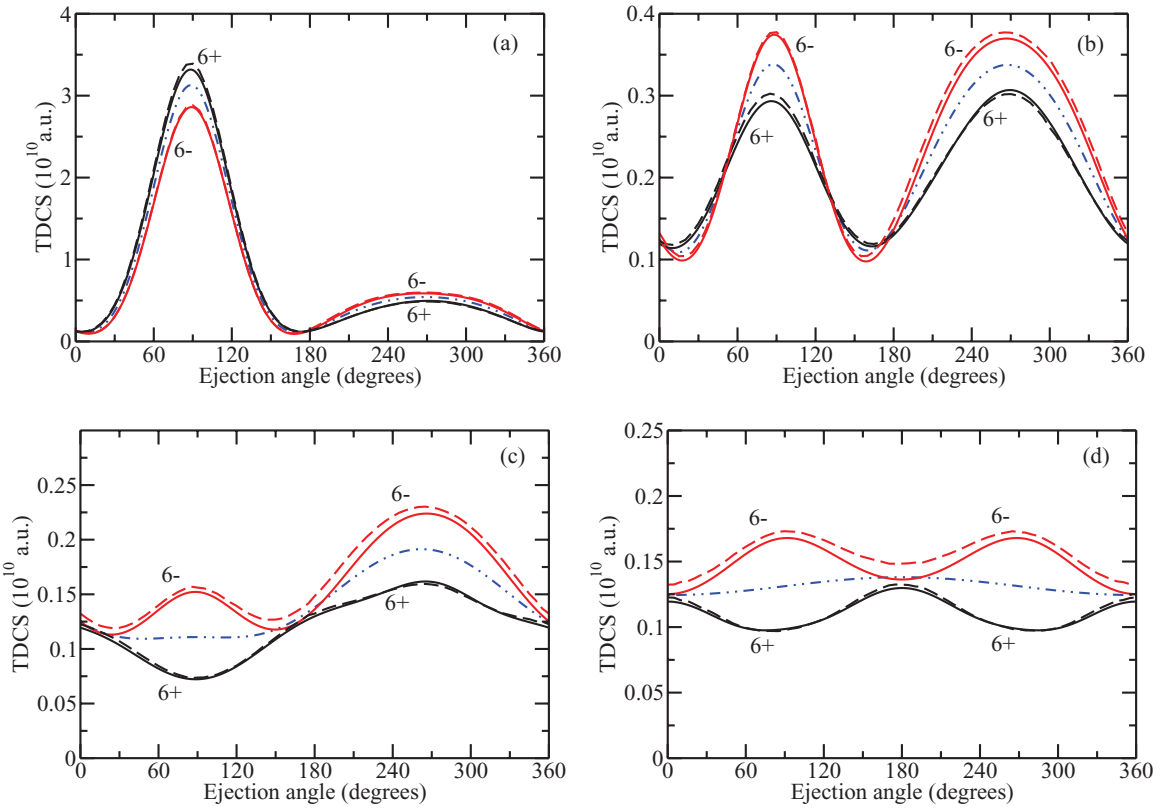

FIG. 1. (Color online) TDCS for C^{6+} and $\overline{C}^{6-}$ at 100 MeV/amu, $q = 0.75$ a.u., and an ejected electron energy of 6.5 eV in planes (a) $\phi = 0°$, (b) $\phi = 60°$, (c) $\phi = 80°$, and (d) $\phi = 90°$. Solid curves, CP approximation; dashed curves, B2 approximation; dash-double-dotted (blue) curve, B1 approximation. Curves (black) labeled with 6+, C^{6+}; curves (red) labeled with 6−, $\overline{C}^{6-}$.

in a single active electron model [three-dimensional (3D) approximation] and in a full two-electron approximation [six-dimensional (6D) approximation]. Both approximations are in accord with each other. From the write-up in [9] we would have expected the results not to have been too different from those (CP) of McGovern *et al.* [1,5]. The CP calculations of McGovern *et al.* [1,5] are somewhat "tighter" than those of Colgan *et al.* in that the impact-parameter range is larger (up to 250 a.u. compared with 90 a.u.), the integration over the projectile path is longer (-10^6 to $+10^6$ a.u. compared with -50 to $+$ over 300 a.u.), the C^{6+}-nucleus interaction is more carefully treated (see the Appendix), and the active electron can access a broader spread of angular momentum states (up to $l = 9$ compared with $l = 3$ in the 3D approximation). We have rerun the CP approximation using the parameters of Colgan *et al.* (impact parameter, projectile path, C^{6+}-nucleus factor, states restricted to $l \leqslant 3$), and while we find differences from the results of McGovern *et al.* [1,5], they do not change greatly what was previously obtained by McGovern *et al.* The parameter choices of Colgan *et al.* do not therefore seem to be the cause of the difference. Having exhausted this possibility, we return to the $C^{6+} + He$ problem to better understand it.

In their paper Colgan *et al.* study, showing some previously unpublished experimental data, how the TDCS alters as the plane of observation is rotated from coplanar geometry into perpendicular plane geometry. In this way one sees how the well-known binary and recoil peaks of coplanar geometry change into what is observed in the perpendicular plane. For coplanar geometry there is no conflict between theory and experiment, and so we can observe in this rotation how the discrepancy could develop. An interesting point that Colgan *et al.* make is that their C^{6+} results are "complementary" to those for 1-keV electron impact ionization of He, i.e., $(e, 2e)$, in the plane perpendicular to the momentum transfer [10]. For both this system and the 100-MeV/amu C^{6+} system, $|Z_P|/v_0$ is close to 0.1, where Z_p is the charge on the projectile and $\boldsymbol{v}_0$ is the incident velocity of the projectile, which suggests that both should be in the same perturbative regime. In the case of e^- impact two peaks are also seen in the plane perpendicular to the momentum transfer near 90° and 270°, as for C^{6+}; see Fig. 3. But, although $|Z_P|/v_0$ may be the same, the sign of the charge matters. To demonstrate the effect of charge sign we consider C^{6+} and e^- together with their antiparticles, $\overline{C}^{6-}$ and e^+. This also enables us to give a physical interpretation of what is happening in the plane perpendicular to the momentum transfer. We shall see that the electron impact results do not just "complement" what we obtain for C^{6+} but "support" it, contrary to the experimental data for C^{6+} and the results of Colgan *et al.* Our vehicle for this intercomparison is the second Born approximation in which we can apply the same approximation to both C^{6+} and e^-. We shall show that this approximation is in good agreement with the impact-parameter CP approximation for C^{6+} and in satisfactory accord with the experimental data for e^- from [10]. Since our second Born approximation is uniformly the same for C^{6+} and e^-, this connection adds strength to our results for C^{6+}.

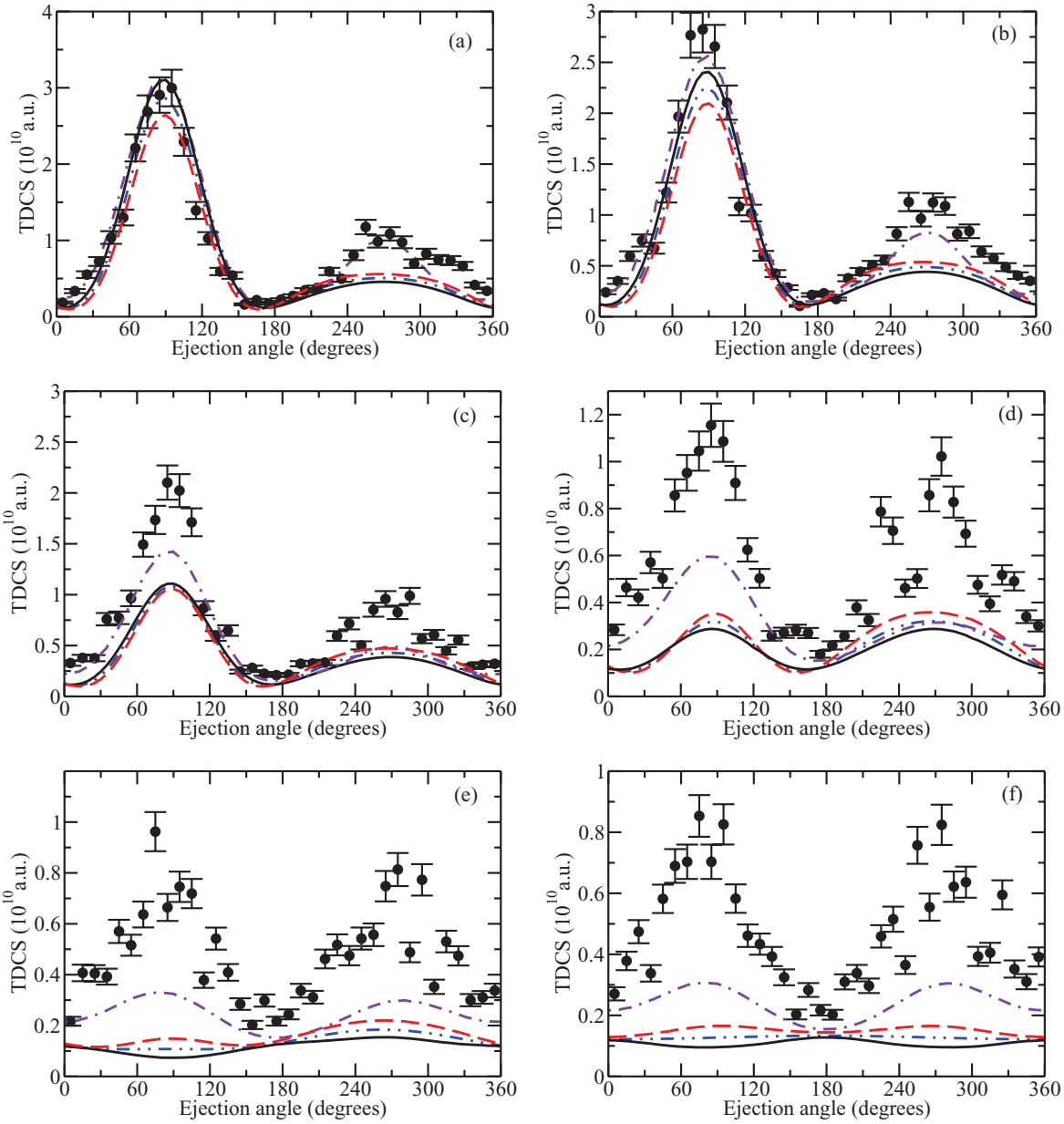

FIG. 2. (Color online) TDCS for C^{6+} and $\overline{C}^{6-}$ at 100 MeV/amu, $q = 0.75$ a.u., and an ejected electron energy of 6.5 eV in planes (a) $\phi = 0°$, (b) $\phi = 20°$, (c) $\phi = 40°$, (d) $\phi = 60°$, (e) $\phi = 80°$, (f) $\phi = 90°$. Solid (black) curve, B2 approximation for C^{6+}; dashed (red) curve, B2 approximation for $\overline{C}^{6-}$; dash-double-dotted (blue) curve, B1 approximation; dash-dotted (violet) curve, 6D TDCC approximation of [9]. Experimental data are from [2] (as quoted in [9])

The structure of this paper is as follows. We begin in Sec. II with a brief description of the first Born, second Born, and impact-parameter coupled-pseudostate approximations used in this paper. Results are presented in Sec. III, first for ionization of He by 100 MeV/amu C^{6+} and $\overline{C}^{6-}$ (Sec. III B). Here the changing pattern of the cross sections is described and interpreted as the plane of observation is rotated about the incident direction (Sec. III B1). This is followed in Sec. III B2 with a comparison to available experimental data. Section III C applies the same high-quality second Born approximation used for C^{6+} and $\overline{C}^{6-}$ to $e^{\pm}$ ionization of He at 1 keV, drawing upon comparisons with experimental data and other second-order calculations to test the approximation and highlighting correlations with the results for $C^{6+}/\overline{C}^{6-}$ impact. Section IV draws all of the arguments and points together into a final conclusion on the C^{6+} + He problem.

Throughout we use atomic units (a.u.) in which $\hbar = m_e = e = 1$. All reported cross sections refer to the laboratory frame of reference [11].

II. THEORY

The scattering amplitude for single ionization of the He atom is

$$f = -\frac{1}{2\pi}\langle e^{i\mathbf{k}_f\cdot\mathbf{R}}\psi_{\kappa}^{-}|V|\Psi_0^{+}\rangle, \qquad (1)$$

where

$$V = Z_P\left(\frac{2}{R} - \frac{1}{|\mathbf{R}-\mathbf{r}_1|} - \frac{1}{|\mathbf{R}-\mathbf{r}_2|}\right). \tag{2}$$

Here $\mathbf{R}$ ($\mathbf{r}_i$) is the position vector of the projectile (ith electron) relative to the He nucleus, Z_P is the charge on the projectile, $\mathbf{k}_f = \mu\boldsymbol{v}_f$, where μ is the reduced mass of the projectile-atom system and $\boldsymbol{v}_f$ is the final velocity of the projectile relative to the target, $\boldsymbol{\kappa}$ is the momentum of the ionized electron relative to the He nucleus, $\psi_{\boldsymbol{\kappa}}^-(\mathbf{r}_1,\mathbf{r}_2)$ is the ionized state of the atom (with ingoing scattered wave boundary conditions), and Ψ_0^+ is the exact scattering wave function for the system.

Once the amplitude (1) has been determined, the TDCS in the laboratory frame is given by [11]

$$\frac{d^3\sigma^L}{dE d\Omega_e d\Omega_p} = \frac{v_f \kappa}{v_0} m_P^2 |f|^2, \tag{3}$$

where m_P is the mass of the projectile. The cross section (3) corresponds to the projectile being scattered into the solid angle $d\Omega_p$ in the laboratory while the ionized electron is ejected into the solid angle $d\Omega_e$ with energy in the range E to $E + dE$. It is assumed that the target atom is initially at rest in the laboratory.

A. Born approximations

In the first Born approximation (B1) the amplitude (1) becomes

$$f^{\text{Born1}} = -\frac{1}{2\pi}\langle e^{i\mathbf{k}_f\cdot\mathbf{R}}\psi_{\boldsymbol{\kappa}}^-|V|e^{i\mathbf{k}_0\cdot\mathbf{R}}\psi_0\rangle, \tag{4}$$

where $\boldsymbol{v}_0$ is the incident velocity of the projectile, $\mathbf{k}_0 = \mu\boldsymbol{v}_0$, and ψ_0 is the initial bound state of the atom. In the second Born approximation (B2) (1) becomes

$$f^{\text{Born2}} = f^{\text{Born1}} + f^{B2}, \tag{5}$$

where the second Born term is

$$f^{B2} = -\frac{\mu}{8\pi^4}\lim_{\eta\to 0+}\sum_n \int d\mathbf{k}\langle e^{i\mathbf{k}_f\cdot\mathbf{R}}\psi_{\boldsymbol{\kappa}}^-|V|e^{i\mathbf{k}\cdot\mathbf{R}}\psi_n\rangle \times \frac{\langle e^{i\mathbf{k}\cdot\mathbf{R}}\psi_n|V|e^{i\mathbf{k}_0\cdot\mathbf{R}}\psi_0\rangle}{k_n^2 - k^2 + i\eta}. \tag{6}$$

In (6) the sum is over all states ψ_n (energy ϵ_n) of the atom, and

$$k_n^2 = k_0^2 + 2\mu(\epsilon_0 - \epsilon_n). \tag{7}$$

We note that the interaction $2Z_P/R$ between the projectile and the atomic nucleus is present in the second Born term for $\psi_n = \psi_0$ and $\psi_n = \psi_{\boldsymbol{\kappa}}^-$ but is otherwise absent and is absent from the first Born term since $\psi_{\boldsymbol{\kappa}}^- \neq \psi_0$. As remarked in Sec. I, the second Born approximation does allow for elastic scattering of the projectile by the atomic nucleus but not with unit probability as assumed in the model of Schulz *et al.* [7].

To evaluate the second Born term (6) we have used the closure approximation [12] and set k_n^2 to an average value $\bar{k}^2$, where

$$\bar{k}^2 = k_0^2 + 2\mu(\epsilon_0 - \bar{\epsilon}) \tag{8}$$

and $\bar{\epsilon}$ is an average energy. The completeness of the atomic states ψ_n is then used to trivially perform the sum over n in (6) and leave a computationally feasible form as described in [13]. Following [1,13–15] we choose $\bar{\epsilon}$ to coincide with the ionization threshold, i.e.,

$$\bar{\epsilon} - \epsilon_0 = 0.9033 \text{ a.u.} \tag{9}$$

In [1] it was shown that for C^{6+} at 100 MeV/amu and an ejected electron energy of 6.5 eV there was little sensitivity to the choice of $\bar{\epsilon}$ within reasonable bounds and that the prescription (9) was reasonable. To calculate (4) and the closured version of (6) we need to know only the initial and final He wave functions, ψ_0 and $\psi_{\boldsymbol{\kappa}}^-$.

B. The impact-parameter coupled-pseudostate approximation

In this approximation [5,11], a set of He eigenstates and pseudostates, ψ_α, is introduced. These states diagonalize the He atomic Hamiltonian H_A:

$$\langle\psi_\alpha|H_A|\psi_\beta\rangle = \epsilon_\alpha\delta_{\alpha\beta}. \tag{10}$$

If the ψ_α approximate a complete set, then (1) may be written

$$f = -\frac{1}{2\pi}\sum_\alpha \langle\psi_{\boldsymbol{\kappa}}^-|\psi_\alpha\rangle\langle e^{i\mathbf{k}_f\cdot\mathbf{R}}\psi_\alpha|V|\Psi_0^+\rangle. \tag{11}$$

Conservation of energy requires that $k_f^2 + 2\mu\epsilon^+ + \mu\kappa^2 = k_0^2 + 2\mu\epsilon_0$, where ϵ^+ is the energy of the residual He^+ ion. Unless deliberately engineered, $k_f^2 + 2\mu\epsilon_\alpha$ will not be equal to $k_0^2 + 2\mu\epsilon_0$, and so the amplitude

$$f_{\alpha 0} \equiv -\frac{1}{2\pi}\langle e^{i\mathbf{k}_f\cdot\mathbf{R}}\psi_\alpha|V|\Psi_0^+\rangle \tag{12}$$

will normally be of energy shell. However, McGovern *et al.* [11] show that, if the pseudostates are chosen so that one state from each angular symmetry has exactly the right energy for conservation, i.e., $\epsilon_\alpha = \epsilon^+ + \kappa^2/2$, then $\langle\psi_{\boldsymbol{\kappa}}^-|\psi_\alpha\rangle$ will be effectively zero for all states ψ_α with $\epsilon_\alpha \neq \epsilon^+ + \kappa^2/2$. Then (11) is limited to only on-energy-shell amplitudes. McGovern *et al.* [11] then go on to establish a connection between the on-energy-shell amplitudes $f_{\alpha 0}$ and the impact parameter approximation. In the latter approximation, the electronic wave function Ψ of the atom, as a function of the time t and the impact parameter $\mathbf{b}$, is expanded in the states ψ_α:

$$\Psi = \sum_\alpha a_\alpha(t,\mathbf{b})e^{-i\epsilon_\alpha t}\psi_\alpha. \tag{13}$$

Substitution of (13) into the time-dependent Schrödinger equation and projection with the ψ_α leads to the coupled equations

$$i\frac{da_\alpha}{dt} = \sum_\beta e^{i(\epsilon_\alpha-\epsilon_\beta)t}\langle\psi_\alpha|V|\psi_\beta\rangle a_\beta, \tag{14}$$

which are solved subject to the boundary conditions $a_\alpha(-\infty,\mathbf{b}) = \delta_{\alpha 0}$. McGovern *et al.* [11] show that, to a very good approximation for heavy projectiles at not too low energies,

$$f_{\alpha 0} = -\frac{iv_0}{2\pi}\int e^{i\mathbf{q}\cdot\mathbf{b}}[a_\alpha(\infty,\mathbf{b}) - \delta_{\alpha 0}]d^2\mathbf{b}, \tag{15}$$

where $\mathbf{q} \equiv \mathbf{k}_0 - \mathbf{k}_f$ is the momentum transfer in the collision and $f_{\alpha 0}$ is on energy shell. Combining (11), (12), and (15) gives the impact-parameter coupled-pseudostate approximation:

$$f = -\frac{iv_0}{2\pi} \sum_{\alpha} \langle \psi_{\kappa}^{-} | \psi_{\alpha} \rangle \int e^{i\mathbf{q}\cdot\mathbf{b}} [a_{\alpha}(\infty, \mathbf{b}) - \delta_{\alpha 0}] d^2\mathbf{b}. \quad (16)$$

It should be emphasized that, although the impact-parameter approach (13) is usually described as "semi-classical," approximation (15) results from a proper wave treatment of the collision; see [11]. Since V contains the term $2Z_P/R$ [see (2)], the approximation includes (coherently) the interaction between the projectile and the He nucleus. This interaction may be removed from Eq. (14) as a phase factor (see the Appendix), but, if this is done, the phase factor (which is a function of b) must be included in the integral (15). For integrated cross sections, on the other hand, which depend only upon $|a_{\alpha}|$ (see [16]), the phase factor is irrelevant, and so the nuclear term $2Z_P/R$ can be totally ignored.

A first Born version of the CP approximation (CPB1) can also be generated by setting $a_{\beta} = \delta_{\beta 0}$ on the right-hand side of (14). Comparison of CPB1 with (4) then gives insight into the validity of the combination, (16), of the approximations (11) and (15), at least at the first Born level.

The He wave functions $\psi_{\alpha}(\mathbf{r}_1, \mathbf{r}_2)$ used here have been calculated as described in [11] in a frozen-core approximation. As indicated in [11], two sets of wave functions have been constructed, one of 75 states and the other of 165 states. Comparison of calculations using the two sets of functions shows that satisfactory convergence of the CP approximation has been obtained for the kinematics considered here. We report only the results of the 165-state approximation. In this approximation the active, i.e., nonfrozen, electron can occupy angular momentum states up to $l = 9$.

III. RESULTS

A. Conventions

In displaying results we adopt the following conventions. We take the Z direction to be the direction of the incident projectile. The incident and scattered projectile define the XZ plane with the scattered projectile coming out on the negative X side. This Cartesian coordinate system is completed with a Y axis to form a right-handed set. We study electron ejection in various planes. For planes containing the Z axis, we adopt the convention that angles are measured from the Z axis in a clockwise direction from 0° to 360°. In the scattering plane this would be a rotation from the Z axis towards the X axis. For e^- and e^+ impact ionization we also consider ejection in a plane perpendicular to the momentum transfer $\mathbf{q}$. For this we introduce a second (primed) right-handed system with X' along the direction of $\mathbf{q}$ and Y′ along the direction of Y. Here we measure angles, 0° to 360°, from the Z' axis rotating towards the Y' axis.

B. Ionization of He by C^{6+} and $\overline{C}^{6-}$

We consider ionization by 100 MeV/amu C^{6+} and $\overline{C}^{6-}$ at a momentum transfer $q = 0.75$ a.u. and for an ejected electron energy of 6.5 eV. Under these conditions, the momentum transfer vector $\mathbf{q}$ lies in the XZ plane and makes an angle $\theta_q = 88.6°$ with the Z axis. We shall study the TDCS in a series of planes obtained by rotating around the Z axis through an azimuthal angle ϕ. The case $\phi = 0°$ (90°) is the XZ (YZ) plane and corresponds to coplanar (perpendicular plane) geometry.

1. Pattern of cross sections

Figure 1 shows the CPB1 and B2 results for both C^{6+} and $\overline{C}^{6-}$. The B1 and B2 approximations have been calculated using the same ground-state wave function ψ_0 as in the CP approximation and the same static-exchange function for ψ_{κ}^{-} [11]. The B1 cross sections are the same for C^{6+} and $\overline{C}^{6-}$. On the scale of Fig. 1 the CPB1 cross section is indistinguishable from the B1 cross section. This indicates the accuracy of approximation (15) and the validity of the pseudostate representation of the ionization, (11), at least at the first Born level. The good agreement seen in Fig. 1 between the CP and B2 approximations justifies the use of second-order perturbation theory under the present kinematics.

In coplanar geometry, Fig. 1(a), there is a clear binary peak near 90° and a recoil peak near 270°. For $\overline{C}^{6-}$ the binary peak in the CP B2 approximation is smaller than in the B1 approximation, and the recoil peak is larger, just as one would expect from $(e,2e)$ [17,18]. The reverse is true for C^{6+}, again as expected from (e^+, e^+e^-) [18]. As ϕ is increased, the binary peak reduces relative to the recoil peak until they are both roughly equal in magnitude at $\phi = 60°$, as in Fig. 1(b) (see also Fig. 2). But a reversal has also taken place in the binary peak region with the C^{6+} peak now lying below the B1 results and the $\overline{C}^{6-}$ peak above. The really interesting transition takes place for ϕ between 60° and 90°. At $\phi = 80°$ [Fig. 1(c)], the binary peak has disappeared from the B1 result, which now shows only a recoil peak. The CP and B2 results for C^{6+} now exhibit a dip in the binary region and a small peak in the recoil region, while $\overline{C}^{6-}$ now has a small peak in the binary region and a more pronounced peak in the recoil area.

At $\phi = 90°$ [Fig. 1(d)], the B1 approximation shows a shallow maximum at 180° (it would be perfectly flat if $\mathbf{q}$ were exactly perpendicular to the YZ plane). Now, we see two minima in the CP and B2 cross sections for C^{6+} near 90° and 270°. The opposite is true for $\overline{C}^{6-}$. This result suggests the following physical interpretation (see [19], however). The B1 approximation allows only for a single impulsive ionizing collision between the projectile and the target electron. Post-collisional interaction (PCI) between the projectile and ionized electron first appears in the B2 approximation and is, of course, also contained in the nonperturbative CP approximation. In the perpendicular plane where the B1 cross section is almost flat, the PCI effect shows up clearly against the "constant" B1 background. In the case of $\overline{C}^{6-}$, the ionized electron is repelled into directions as far away as possible from the projectile path, hence the minima at 0° and 180° and maxima at 90° and 270°. For C^{6+}, the reverse is true, with electrons appearing preferentially in the directions of 0° (= 360°) and 180°.

The patterns shown in Fig. 1(d) are in agreement with the Glauber, second Born, and CDW eikonal initial state (CDW-EIS) calculations of Voitkiv *et al.* [3] on C^{6+} and $\overline{C}^{6-}$ collisions with H at 100 MeV/amu, an ejected electron energy of 10 eV, and a momentum transfer q of 1 a.u. Voitkiv *et al.* also looked at

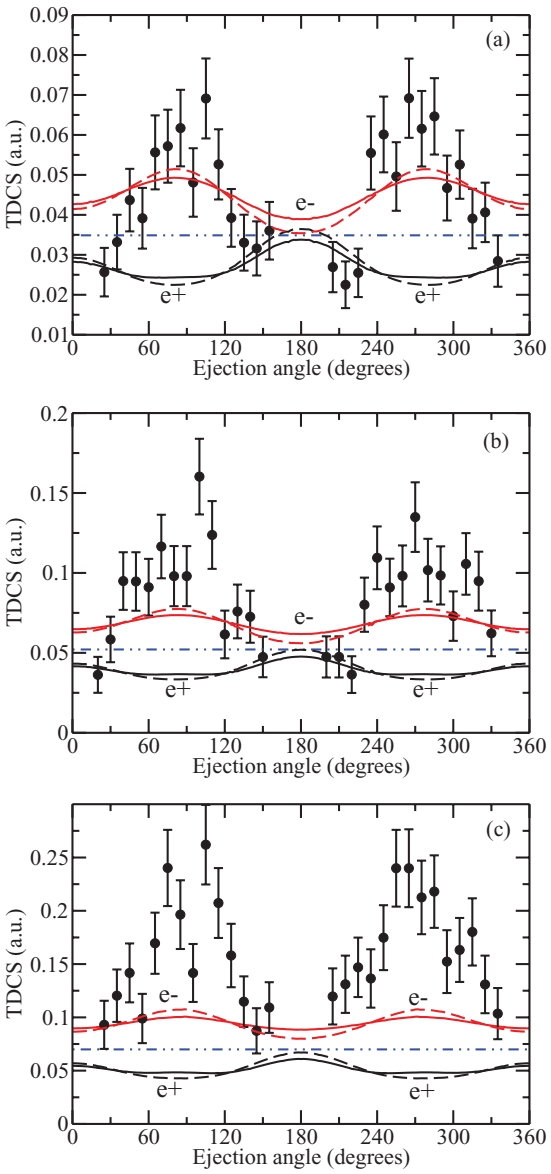

FIG. 3. (Color online) TDCS in the plane perpendicular to the momentum transfer **q** for $e^{\pm}$ impact at 1 keV and an ejected electron energy of 10 eV for momentum transfers q of (a) 1.0 a.u., (b) 0.75 a.u., and (c) 0.50 a.u. Solid curves, B2 approximation; dashed curves, B2POL approximation; dash-double-dotted (blue) curve, B1 approximation. Curves labeled e^- (red), e^+ (black). Experimental data are from [10].

He but, being concerned about the quality of their approximate He wave functions, were wary of their results. While these results were not explicitly reported, Voitkiv *et al*. say that they generally gave agreement with the pattern for H, although, depending upon the choice of wave function parameters, they could be occasionally different. The wave functions used in the present paper are of a very much higher quality than those employed by Voitkiv *et al*.

That the structures seen in Fig. 1(d) are reproduced in a range of approximations for both He and H and that there is a sensible physical interpretation of the results are very strong support for the patterns seen in Fig. 1(d) and a contradiction of the recent results of Colgan *et al*. [9].

2. *Comparison with experiment*

In Fig. 2 we compare our B1 and B2 calculations with the experimental data of Schulz *et al*. [2] (as quoted in [9]) for C^{6+} impact. For this we use the best He wave functions at our disposal. In calculating f^{Born1} of (4) we take ψ_0 to be the accurate ground-state wave function of Kinoshita [20] (energy accurate to six significant figures) and ψ_f to be the 60-state coupled-pseudostate wave function of [21] for electron scattering by $He^+(1s)$. For f^{B2} of (6) we follow [13,21] and take ψ_0 to be the ground-state wave function of Byron and Joachain [22] and ψ_f to be a three-state $1s$-$2s$-$2p$ close-coupling wave function for e^- + $He^+(1s)$ scattering. In [1] a comparison was made between B1 and B2 results evaluated with these wave functions and the corresponding calculations of Fig. 1 for C^{6+} impact in coplanar and perpendicular plane geometry. The differences seen in these two geometries, which were typically less than 10% (and mostly came from the f^{Born1} term), reflect the general degree of agreement between the two sets of wave functions in the other geometries of Fig. 2, for both C^{6+} and $\overline{C}^{6-}$.

In coplanar geometry [$\phi = 0^\circ$; Fig. 2(a)], both B1 and B2 calculations are in good, but not perfect, agreement with the experimental data for C^{6+} in the angular range up to 240°. Beyond, in the recoil peak region, experiment separates from theory. With increasing ϕ the separation between theory and experiment grows, with differences in the binary peak already appearing at $\phi = 20^\circ$ [Fig. 2(b)]. While experiment continues to show two peaks near 90° and 270° for all ϕ, the B2 calculation for C^{6+} transforms, as seen in Fig. 1, from two peaks for ϕ up to 60° into two dips at $\phi = 90^\circ$ [Fig. 2(f)]. The results for $\overline{C}^{6-}$ show two peaks near 90° and 270° for all ϕ but, as explained in Sec. III B1, the physical understanding of these peaks changes with ϕ. At $\phi = 0^\circ$, they are the familiar binary and recoil peaks. At $\phi = 90^\circ$, they correspond to PCI effects in which the ionized electron tries to move as far away as possible from the projectile path.

Figure 2 also shows the 6D TDCC results of Colgan *et al*. [9], which are seen to be in better accord with experiment, in particular, showing much better agreement in the recoil peak region for $\phi = 0^\circ$ and 20° and, as in experiment, retaining the two-peak structure near 90° and 270° for the whole range of ϕ up to 90°. However, experiment gives substantially larger cross sections than the TDCC results with increasing ϕ, although the discrepancy in magnitude is less than for the B2 results.

The comparisons with experiment made here lack allowance for experimental resolutions, which, no doubt, would explain a lot of the differences seen in Fig. 2. Indeed, Fiol *et al*. [4] explained all of the differences between their theories (B1 and CDW) and experiment in coplanar and perpendicular plane geometry as experimental resolution. However, Dürr *et al*. [6] contradicted this analysis and, in a different analysis, claimed that two peaks near 90° and 270° still remained in perpendicular plane geometry after resolution matters were settled. The question addressed here, therefore, is whether there are peaks or dips at 90° and 270° for $\phi = 90^\circ$ in the unconvoluted (with experimental resolutions) TDCS. On that our calculations, giving dips, disagree strongly with those of Colgan *et al*.

C. Ionization of He by e^- and e^+

In this section we apply the B2 and B1 approximations described in Sec. III B2 to e^- and e^+ ionization of He at an impact energy of 1 keV. We compare our results with $(e,2e)$ measurements from [10] which have been made for an ejected electron energy of 10 eV and momentum transfers of $q = 0.5$, 0.75, and 1.0 a.u. This system, for which $|Z_P|/v_0 = 0.117$ and which has similar ejected electron energy and momentum transfers, is comparable to the case of C^{6+} studied in Sec. III B ($|Z_P|/v_0 = 0.094$). Three geometries are considered: coplanar, perpendicular plane (i.e., YZ plane), and the plane perpendicular to the momentum transfer $\mathbf{q}$. Whereas the latter two geometries were approximately the same for the previously considered C^{6+} ($\theta_q = 88.6^\circ$), it is not so for the $e^\pm$ impact studied here.

The e^- data have already been compared to two second-order calculations, the plane-wave second Born approximation combined with a convergent R matrix with pseudostate expansion (PWB2-RMPS) and second-order distorted-wave model (DWB2), in [10]. The PWB2-RMPS approximation is similar to the B2 calculation but differs in detail [23,24]. Like the B2 calculation it uses an average $\bar{k}$ ($= \sqrt{k_0 k_f}$) to calculate f^{B2} [see (6)], but instead of applying closure to sum over the intermediate states ψ_n, it replaces them with pseudostates constructed out of the R-matrix basis used to calculate ψ_0 and $\psi_{\mathbf{k}}^-$. Closure is more accurate since it assumes exact ψ_n. However, the PWB2-RMPS calculation uses the same high-quality ψ_0 and $\psi_{\mathbf{k}}^-$ to evaluate f^{B2} as it employs for f^{Born1}, whereas the B2 calculation uses simpler functions for the second-order term. One potentially important difference, however, is that the PWB2-RMPS calculation retains only the pole-term contribution to the propagator in (6), i.e., writing

$$\frac{1}{\bar{k}^2 - k^2 + i\eta} = \mathrm{P}\frac{1}{\bar{k}^2 - k^2} + \frac{i\pi}{2\bar{k}}\delta(k - \bar{k}), \qquad (17)$$

where P stands for principal value, the PWB2-RMPS approximation neglects the principal-value term. To see the effect of this further approximation we have also performed calculations retaining only the pole term in f^{B2}; this approximation we label B2POL. In the DWB2 approximation [10,25] the plane waves in (6) describing the projectile in the initial and final states are replaced by distorted waves in which the projectile electron feels distorting potentials representing the static field of the atom; the projectile in the intermediate states is still treated as a plane wave. Instead of the closure approximation, pseudostates are used to approximate the intermediate states ψ_n in (6). However, the initial and final wave functions, ψ_0 and $\psi_{\mathbf{k}}^-$, of the atom are of lower quality than those employed in the PWB2-RMPS calculation or in the first-order term of the B2 calculation. Overall, our B2 results for e^- are very comparable to these earlier second-order calculations, but there still remain some useful observations to make.

In Fig. 3 we show results in the plane perpendicular to $\mathbf{q}$. In this plane the B1 cross section is constant, and deviations from this constant value reflect the importance of higher-order terms in the Born series. Here we see marked agreement with the pattern of Figs. 1(d) and 2(f), showing that the same physics, PCI, is operative. Different from Fig. 2(f), however, is the agreement between experiment and theory for e^- at $q = 0.75$ and 1.0 a.u. At $q = 0.5$ a.u. [Fig. 3(c)], experiment drifts away from theory somewhat, but both theory and experiment still agree that there are peaks near 90° and 270°. By contrast, the theoretical results for e^+ show dips at these angles in accord with the theoretical results for C^{6+} in Figs. 1(d) and 2(f) and contrary to experiment in Fig. 2(f). The measurements shown in Fig. 3 are on a stronger footing than those for C^{6+} [10] since both the scattered and ejected electrons are detected, while for C^{6+} the motion of the scattered projectile has to be inferred from the momentum of the recoil ion and therefore, for example, depends upon the target temperature. Furthermore, experimental resolutions do not appear to be as big a problem in the $(e,2e)$ case. Our B1 cross section differs by less than 3% from the PWB1-RMPS cross section of [10], and the comparison between the B2 and B2POL approximations indicates that neglect of the principal-value term in (17) is not a significant approximation in this geometry.

Figure 4 shows cross sections in the perpendicular plane (the YZ plane). Although this plane was a good approximation for the plane perpendicular to $\mathbf{q}$ for C^{6+}, it is not quite so for $(e,2e)$, where $\theta_q = 78.1^\circ$, 76.0°, and 71.0° [26] for $q = 1.0$, 0.75, and 0.50 a.u., respectively. This can be seen from the variation away from a constant value of the B1 cross section. This variation increases as q is reduced from 1.0 to 0.50 a.u. At $q = 1.0$ a.u. [Fig. 4(a)] the B2 cross section for e^- shows "shoulders" near 80° and 280°, while, correspondingly, the e^+ cross section shows dips near 60° and 300°; this is the PCI effect showing up against the B1 background. The experimental data exhibit clear peaks near 75° and 285° but suggest a dip at 180°, contrary to the B2 cross section, which has a peak at this angle. However, the B2POL cross section shows a shallow minimum at 180° and slightly enhanced shoulders, making it in marginally better agreement with experiment. Comparing with [10], the B2 cross section resembles the DWB2 results, while the B2POL cross section reproduces the shape of the PWB2-RMPS results. In [10] the difference in form between the DWB2 and PWB2-RMPS methods was attributed to the differing quality of wave functions. Since the DWB2 approximation retains the principal-value term of (17), we now see that the difference is not due to wave functions but to the neglect of that term, which, fortuitously, improves the agreement with experiment. However, the PWB2-RMPS method is similar to the nonperturbative convergent close-coupling (CCC) approximation shown in [10], especially in the flat region around 180°. This suggests that higher-order Born terms may cancel the principal-value contribution to the B2 approximation, at least in the case of Fig. 4(a).

At $q = 0.75$ a.u. [Fig. 4(b)], there remains a nuance of shoulders in the e^- B2 and B2POL cross sections near 75° and 285° and a much more definite dip in the e^+ cross sections near 60° and 300°. Now all theories (B2, B2POL, DWB2, PWB2-RMPS, CCC) agree that there is a peak in the e^- cross section at 180°, while experiment still seems to indicate a dip. By $q = 0.50$ a.u. [Fig. 4(c)], there is no evidence of shoulders in the e^- B2 and B2POL cross sections, and although there is a dip in the cross section for e^+ near 70° and 290°, such a dip is also evident in the impulsive, no PCI, B1 cross section. Experiment continues to suggest that there may not be a peak at 180°, contrary to all of the theories.

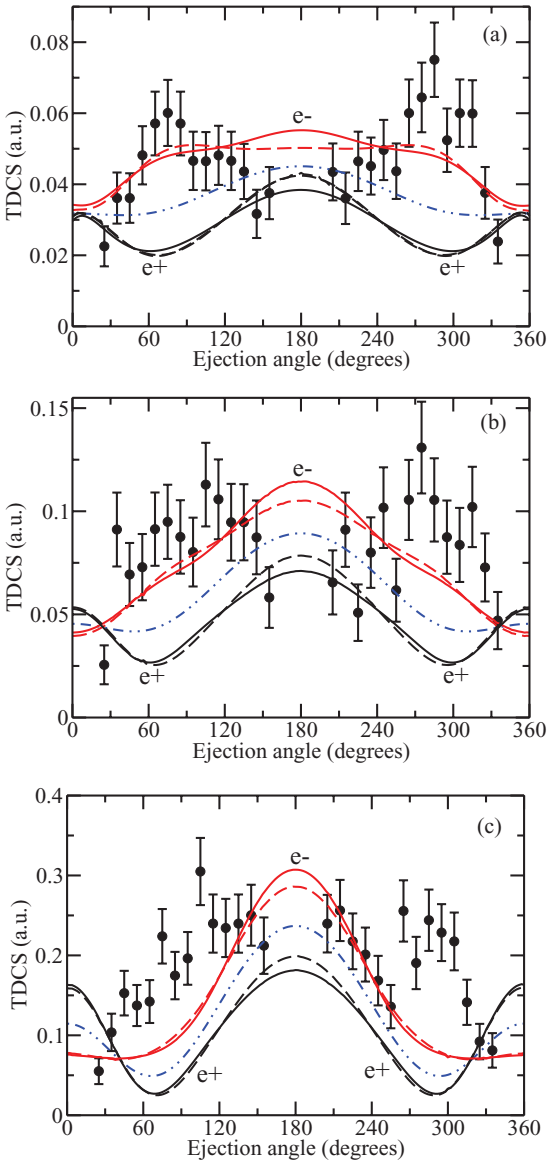

FIG. 4. (Color online) TDCS in the perpendicular YZ plane for $e^{\pm}$ impact at 1 keV and an ejected electron energy of 10 eV for momentum transfers q of (a) 1.0 a.u., (b) 0.75 a.u., and (c) 0.50 a.u. Solid curves, B2 approximation; dashed curves, B2POL approximation; dash-double-dotted (blue) curve, B1 approximation. Curves labeled e^- (red), e^+ (black). Experimental data are from [10].

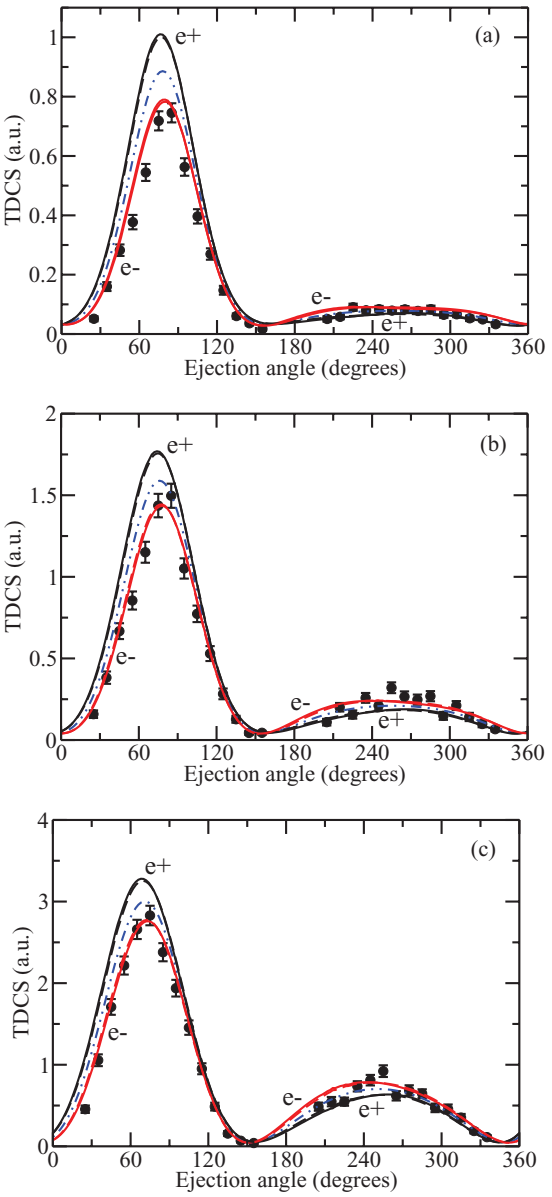

FIG. 5. (Color online) TDCS in coplanar geometry for $e^{\pm}$ impact at 1 keV and an ejected electron energy of 10 eV for momentum transfers q of (a) 1.0 a.u., (b) 0.75 a.u., and (c) 0.50 a.u. Solid curves, B2 approximation; dashed curves, B2POL approximation; dash-double-dotted (blue) curve, B1 approximation. Curves labeled e^- (red), e^+ (black). Experimental data are from [10].

Figure 5 illustrates the quality of agreement that can be obtained between theory and experiment in the more "robust" coplanar geometry. It also shows that the principal-value term of (17) is not important in this geometry; it is almost impossible to see the difference between B2 and B2POL. Figure 5 illustrates again (see [17,18]) that, compared with the B1 results, the binary peak is reduced (enhanced) for e^- (e^+), the opposite being true for the recoil peak; also, the binary and recoil peaks are rotated away from (towards) the outgoing projectile for e^- (e^+).

IV. CONCLUSIONS

Using exactly the same second-order B2 approximation, we have shown that the same pattern of cross sections, in the plane perpendicular to the momentum transfer **q** and under comparable dynamical conditions, is obtained for C^{6+} and $\overline{C}^{6-}$, on the one hand, as for e^+ and e^-, respectively, on the other hand. In the case of e^- the B2 results are in satisfactory, although not perfect, accord with experiment, as are other theories. In the case of C^{6+} there is complete disagreement between the B2 approximation and experiment in the plane (approximately) perpendicular to **q**. Here experiment displays two pronounced peaks near 90° and 270°, while the B2 approximation exhibits shallow minima at these positions. According to the B2 approximation, peaks are predicted for negatively charged projectiles, $\overline{C}^{6-}$ and e^-, but dips are predicted for positively charged projectiles, C^{6+} and e^+. This

difference, we suggest, is a PCI effect in which the ionized electron is repelled by a negatively charged projectile and attracted by a positively charged one.

That dips rather than peaks near 90° and 270° are to be expected for C^{6+} at 100 MeV/amu is predicted by a range of approximations, viz., B2, CP, CDW, CDW-EIS, and Glauber. Unique among sophisticated approximations, the TDCC approximation of Colgan *et al.* [9] predicts peaks. Colgan *et al.* remark that they treat the projectile classically and therefore incoherently and that this might be the cause of the difference. However, this does not necessarily follow. In deriving the CP approximation (16), McGovern *et al.* [11] use such a straight-line impact parameter approximation but apply it as an approximation to a full wave treatment. The resulting CP approximation is fully coherent and quantal and in agreement with the B2 results for 100 MeV/amu C^{6+}.

While experimental resolution is, at least, a large part of the discrepancy between the B2 and CP approximations and experiment, incoherence of the experimental beam is possibly the rest, a point made in a recent paper by Egodapitiya *et al.* [27]. Recalling that the wavelength of a particle of mass M moving with speed v_0 is (nonrelativistically) $2\pi/(Mv_0)$, we see that a C^{6+} will have a wavelength 1/(21,875) times smaller than that of an electron with the same velocity. This very much shorter wavelength makes it much more difficult to get a coherent beam at the target, which is especially important if deflection of the projectile is to be measured. We note that the wavelength of a 100 MeV/amu C^{6+} is (nonrelativistically) 1/(162,000) times smaller than that of a 1-keV e^-, possibly explaining the agreement of the B2 results with experiment for e^- but not for C^{6+}. Other possibilities, such as wave-function quality, excitation of the He^+ ion, and relativistic effects, have been eliminated by McGovern *et al.* [1] as viable explanations for the peaks in the C^{6+} perpendicular plane experimental data at 100 MeV/amu.

ACKNOWLEDGMENTS

We are indebted to Y. Popov, K. Kouzakov, and S. Zaytsev for useful discussions on this problem.

APPENDIX

In the impact-parameter approximation the electronic wave function Ψ for the projectile + He system satisfies the time-dependent Schrödinger equation

$$(H_A + V)\,\Psi = i\frac{\partial \Psi}{\partial t}, \tag{A1}$$

where, from (2),

$$V = Z_P\left(\frac{2}{R} - \frac{1}{|\mathbf{R}-\mathbf{r}_1|} - \frac{1}{|\mathbf{R}-\mathbf{r}_2|}\right) \tag{A2}$$

and $\mathbf{R} = \mathbf{b} + \boldsymbol{v}_0 t$. The interaction $V_{\rm nuc} = 2Z_P/R$ between the projectile and the He nucleus may be removed from (A1) by taking

$$\Psi = \exp\left(-\frac{i}{v_0}\int^z \frac{2Z_P}{\sqrt{b^2+z'^2}}dz'\right)\Phi, \tag{A3}$$

where $z = v_0 t$. Then (A1) becomes

$$(H_A + V_{\rm elect})\,\Phi = i\frac{\partial \Phi}{\partial t}, \tag{A4}$$

where $V_{\rm elect} = V - V_{\rm nuc}$. If (A4) is integrated between times $-t_0$ and $+t_1$, then the corresponding Ψ is

$$\Psi = e^{i\delta(b)}\Phi, \tag{A5}$$

where

$$\delta(b) = -\frac{2Z_P}{v_0}\ln\left\{\frac{\left[z_0+\sqrt{b^2+z_0^2}\right]\left[z_1+\sqrt{b^2+z_1^2}\right]}{b^2}\right\} \tag{A6}$$

and $z_i = v_0 t_i$ $(i = 0,1)$.

Colgan *et al.* [9] use a phase

$$\delta(b) = \frac{2Z_P Z_{\rm eff}}{v_0}\ln(v_0 b), \tag{A7}$$

where the nuclear interaction is $Z_P Z_{\rm eff}/R$. This can be obtained from (A6) in the limit of large z_0 and z_1 when (A6) becomes

$$-\frac{2Z_P}{v_0}\ln\left(4v_0^2 z_0 z_1\right) + \frac{4Z_P}{v_0}\ln(v_0 b). \tag{A8}$$

If z_0 and z_1 are chosen independent of b, then the first term in (A8) may be neglected as an overall phase factor, leaving the result (A7) with $Z_{\rm eff} = 2$.

An important point to note is that, asymptotically in R, $V_{\rm nuc}$ and $V_{\rm elect}$ are Coulombic, while V goes to zero at least as fast as $1/R^2$. We must therefore be careful that, for any finite z_0 and z_1, we implement the nuclear phase $\delta(b)$ with sufficient accuracy. The result (A6) is exact, but (A7) is only approximate and depends upon the choice of z_0 and z_1 being independent of b and sufficiently large.

[1] M. McGovern, C. T. Whelan, and H. R. J. Walters, Phys. Rev. A **82**, 032702 (2010).
[2] M. Schulz, R. Moshammer, D. Fisher, H. Kollmus, D. H. Madison, S. Jones, and J. Ullrich, Nature (London) **422**, 48 (2003).
[3] A. B. Voitkiv, B. Najjari, and J. Ullrich, J. Phys. B **36**, 2591 (2003).
[4] J. Fiol, S. Otranto, and R. E. Olson, J. Phys. B **39**, L285 (2006).
[5] M. McGovern, D. Assafrão, J. R. Mohallem, C. T. Whelan, and H. R. J. Walters, Phys. Rev. A **81**, 042704 (2010).
[6] M. Dürr, B. Najjari, M. Schulz, A. Dorn, R. Moshammer, A. B. Voitkiv, and J. Ullrich, Phys. Rev. A **75**, 062708 (2007).
[7] M. Schulz, M. Dürr, B. Najjari, R. Moshammer, and J. Ullrich, Phys. Rev. A **76**, 032712 (2007).

[8] M. Schulz, Phys. Scr. **80**, 068101 (2009).
[9] J. Colgan, M. S. Pindzola, F. Robicheaux, and M. F. Ciappina, J. Phys. B **44**, 175205 (2011).
[10] M. Dürr, C. Dimopoulou, B. Najjari, A. Dorn, K. Bartschat, I. Bray, D. V. Fursa, Z. Chen, D. H. Madison, and J. Ullrich, Phys. Rev. A **77**, 032717 (2008).
[11] M. McGovern, D. Assafrão, J. R. Mohallem, C. T. Whelan, and H. R. J. Walters, Phys. Rev. A **79**, 042707 (2009).
[12] H. R. J. Walters, Phys. Rep. **116**, 1 (1984).
[13] P. J. Marchalant, C. T. Whelan, and H. R. J. Walters, J. Phys. B **31**, 1141 (1998).
[14] H. Ehrhardt, M. Fischer, K. Jung, F. W. Byron Jr., C. J. Joachain, and B. Piraux, Phys. Rev. Lett. **48**, 1807 (1982).
[15] J. Marchalant, B. Rouvellou, J. Rasch, S. Rioual, C. T. Whelan, A. Pochat, D. H. Madison, and H. R. J. Walters, J. Phys. B **33**, L749 (2000).
[16] M. McGovern, D. Assafrão, J. R. Mohallem, C. T. Whelan, and H. R. J. Walters, Phys. Rev. A **81**, 032708 (2010).
[17] E. P. Curran and H. R. J. Walters, J. Phys. B **20**, 337 (1987).
[18] M. Brauner, J. S. Briggs, and H. Klar, J. Phys. B **22**, 2265 (1989).
[19] Voitkiv *et al*. [3] assign the structures of Fig. 1(d) to the projectile-nucleus interaction. They note that switching off this interaction in the Glauber, second Born, and CDW-EIS approximations leads to a "flat" cross section similar to the B1 approximation (in fact, identical for Glauber). However, we would argue that this changes the physical problem totally. Now, the projectile sees not a heavy neutral atom but a light negatively charged target. Our view is that, while the projectile-nucleus interaction is essential for a correct description, it is not in itself the cause of the peaks.
[20] T. Kinoshita, Phys. Rev. **105**, 1490 (1957).
[21] P. J. Marchalant, J. Rasch, C. T. Whelan, D. H. Madison, and H. R. J. Walters, J. Phys. B **32**, L705 (1999).
[22] F. W. Byron Jr. and C. J. Joachain, Phys. Rev. **146**, 1 (1966).
[23] R. H. G. Reid, K. Bartschat, and A. Raeker, J. Phys. B **31**, 563 (1998); **33**, 5261 (2000).
[24] Y. Feng and K. Bartschat, J. Phys. B **34**, L19 (2001).
[25] Z. Chen and D. H. Madison, J. Phys. B **38**, 4195 (2005).
[26] These numbers disagree with those quoted by Dürr *et al*. [10], namely, 87°, 85°, and 79°, respectively, which are not consistent with the position of the binary peak in the coplanar cross sections shown in their paper.
[27] K. N. Egodapitiya, S. Sharma, A. Hasan, A. C. Laforge, D. H. Madison, R. Moshammer, and M. Schulz, Phys. Rev. Lett. **106**, 153202 (2011).